Molecular Crystals and Liquid Crystals

Publication details, including instructions for authors and subscription information:
http://www.tandfonline.com/loi/gmcl20

DIRECTOR CONFIGURATION OF A NEMATIC LIQUID CRYSTAL AROUND A SPHERICAL PARTICLE: NUMERICAL ANALYSIS USING ADAPTIVE MESH REFINEMENT

Jun-ichi Fukuda [a], Makoto Yoneya [a] & Hiroshi Yokoyama [a b]

[a] Yokoyama Nano-structured Liquid Crystal Project, ERATO, Japan Science and Technology Corporation, 5-9-9 Tokodai, Tsukuba 300-2635, Japan

[b] Nanotechnology Research Institute, AIST, 1-1-4 Umezono, Tsukuba 305-8568, Japan

Version of record first published: 07 Jan 2010

To cite this article: Jun-ichi Fukuda, Makoto Yoneya & Hiroshi Yokoyama (2004): DIRECTOR CONFIGURATION OF A NEMATIC LIQUID CRYSTAL AROUND A SPHERICAL PARTICLE: NUMERICAL ANALYSIS USING ADAPTIVE MESH REFINEMENT, Molecular Crystals and Liquid Crystals, 413:1, 221-229

To link to this article: http://dx.doi.org/10.1080/15421400490437141

Mol. Cryst. Liq. Cryst., Vol. 413, pp. 221/[2357]–229/[2365], 2004

ISSN: 1542-1406 print/1563-5287 online
DOI: 10.1080/15421400490437141

Taylor & Francis
Taylor & Francis Group

DIRECTOR CONFIGURATION OF A NEMATIC LIQUID CRYSTAL AROUND A SPHERICAL PARTICLE: NUMERICAL ANALYSIS USING ADAPTIVE MESH REFINEMENT

Jun-ichi Fukuda and Makoto Yoneya,
Yokoyama Nano-structured Liquid Crystal Project, ERATO,
Japan Science and Technology Corporation, 5-9-9 Tokodai,
Tsukuba 300-2635, Japan

Hiroshi Yokoyama
Yokoyama Nano-structured Liquid Crystal Project, ERATO,
Japan Science and Technology Corporation, 5-9-9 Tokodai,
Tsukuba 300-2635, Japan
and
Nanotechnology Research Institute, AIST, 1-1-4 Umezono,
Tsukuba 305-8568, Japan

We investigate numerically the orientational configuration of a nematic liquid crystal around a spherical particle. The use of adaptive mesh refinement scheme proves quite useful to overcome the numerical difficulty arising from large scale difference between a particle and a topological defect. Our scheme reproduces successfully the hedgehog and the Saturn ring configurations that have been observed experimentally. To demonstrate that dynamical behaviors can also be investigated using our scheme, we present a simulation result which exhibits a transition from a hedgehog to a Saturn ring under the application of an external field.

Keywords: adaptive mesh refinement; colloid; nematic liquid crystal; topological defect

INTRODUCTION

Liquid crystal colloids and emulsions have attracted a great deal of interest in fundamental science as well as in technology as a new composite

Address correspondence to Jun-ichi Fukuda, Yokoyama Nano-Structured Liquid Crystal Project, ERATO, Japan Science and Technology Corporation, 5-9-9 Tokodai, Tsukuba 300-2635, Japan.

material [1–3]. They also provide an interesting problem on topological defects: what kind of defects will be formed due to the inclusion of colloidal particles or droplets and what determines their structures? Experimentally observed defects include a hyperbolic hedgehog [2,4], a Saturn ring [5,6], and boojum defects [4] (Fig. 1) depending on the type and strength of anchoring of the droplet surfaces.

Although several theoretical and numerical studies [7–14] have been devoted to the understanding of the director and defect configuration around particles or droplets, all of the numerical studies suffered from a numerical difficulty resulting from a large difference between two characteristic length scales: the size of a particle and that of the core of topological defects. In the previous studies a direct treatment of a topological defect was not possible and the evaluation of the elastic energy was accomplished by introducing a cutoff. Moreover, pinning of topological defect due to an insufficient numerical resolution made it almost impossible to simulate a dynamical behavior of topological defects.

In our previous studies [15,16] we have implemented an adaptive mesh refinement scheme to investigate the orientation profile of a nematic liquid crystal around a spherical particle. It has proven to be quite an efficient and powerful scheme and together with employing a description in terms of a tensor order parameter, it enables a direct treatment of a topological defect. With the aid of a fine numerical resolution achieved by an adaptive mesh refinement we could observe a ring-like fine structure of a hyperbolic hedgehog. Since in our previous paper only a hedgehog configuration was discussed in a three-dimensional system, in this article we first show that our scheme reproduces successfully a Saturn-ring configuration as well as a hedgehog. Moreover, to show that our scheme can be applied to the investigation of the dynamics of topological defects, we present simulation results which exhibit transformation of a hedgehog to a Saturn ring under an external field recently observed in experiments [17].

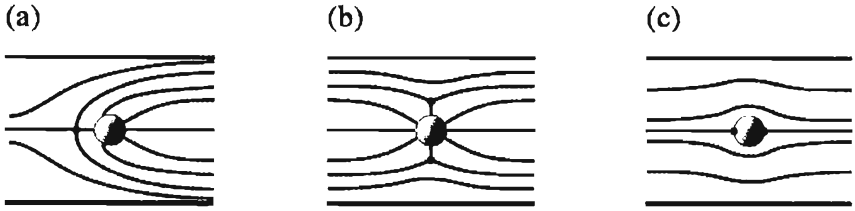

FIGURE 1 Schematic illustrations of (a) a hyperbolic hedgehog, (b) a Saturn ring, and (c) boojum defects.

MODEL

In this section we describe our numerical system. Instead of a director $\boldsymbol{n}$, we use a second rank traceless tensor $Q_{ij}(\boldsymbol{r})$ to specify the orientational order of the system at point $\boldsymbol{r}$. We note that the employment of a second-rank tensor is consistent with the head-tail symmetry of a nematic.

We write the free energy density in the bulk as $f = f_{LdG}(Q_{ij}) + f_{el}(Q_{ij}, \partial_i) + f_{ext}(Q_{ij}, \tilde{H}_i)$, where $f_{LdG}(Q_{ij})$ is the local energy, f_{el} is the elastic energy of orientational distortion, and f_{ext} is the energy due to an external (magnetic or electric) field $\tilde{H}$ The local energy $f_{LdG}(Q_{ij})$ is expressed in terms of the Landau-de Gennes expansion:

$$f_{LdG} = -\frac{1}{2}A\mathrm{TrQ}^2 + \frac{1}{3}B\mathrm{TrQ}^3 + \frac{1}{4}C(\mathrm{TrQ}^2)^2 + \lambda\mathrm{TrQ}. \tag{1}$$

Here $\mathrm{TrQ} = Q_{ii}$, $\mathrm{TrQ}^2 = Q_{ij}Q_{ji}$ and so on and summations over repeated indices are implied. The last term ensures the tracelessness of the order parameter, i.e., $\mathrm{TrQ} = 0$, with λ being a Lagrange multiplier. We set the phenomenological coefficients as $C = -B = 3A$ so that a uniaxial configuration $Q_{ij} = Q_{bulk}(m_i m_j - (1/3)\delta_{ij})$, with $Q_{bulk} = 1$ and $\boldsymbol{m}$ being an arbitrary unit vector, minimizes the local energy. We note that this is not the unique choice to satisfy the above condition and that a difference of the coefficients may affect the fine, possibly biaxial, structure of the defect core, which will be a subject of future studies. We adopt a following simple one-constant form for the elastic energy:

$$f_{el} = \frac{1}{2}L_1\partial_k Q_{ij}\partial_k Q_{ij}. \tag{2}$$

We write the energy due to an external field as

$$f_{ext} = -\tilde{H}_i\tilde{H}_j\frac{Q_{ij}}{\sqrt{\mathrm{TrQ}^2}}. \tag{3}$$

The minus sign indicates that in the presence of an external field the director tends to be parallel to the field. We have divided the usual expression $-\tilde{H}_i\tilde{H}_jQ_{ij}$ by $\sqrt{\mathrm{TrQ}^2}$ because otherwise the orientational profile Q_{ij} that minimizes the bulk energy $f_{LdG} + f_{ext}$ will change according to the variation of the external field. The dimensionless field $\tilde{H}$ is associated with a dimensional one H as $\tilde{H}^2 = \Delta_\chi H^2/\sqrt{6}$, with Δ_χ being the anisotropy of the susceptibility. We notice that there exist two characteristic lengths in our system apart from the particle radius R_0 and we will express them as dimensionless quantities in units of R_0. One is the nematic coherence length $\xi = \sqrt{L_1/A}/R_0$ and the other is the magnetic coherence length $\xi_H = \sqrt{L_1/\tilde{H}^2}/R_0$. We also

note that ξ can be regarded as the size of the core of a topological defect and that ${\xi_H}^{-1}$ is proportional to $\tilde{H}$ from the definition.

Although some of the previous studies [7–9,11,12] dealt with the case of finite anchoring strength on the particle surface, for the simplicity of numerical calculations we assume rigid homeotropic anchoring and set $Q_{ij} = Q_s(n_i n_j - (1/3)\delta_{ij})$ with $Q_s = Q_{bulk} = 1$ and $\boldsymbol{n}$ being a unit vector normal to the particle surface. Therefore surface energy does not appear in our numerical system. We consider a case where a particle is immersed in a uniform nematic aligned along the z-axis and at infinity we impose $Q_{ij} = Q_{bulk}(e_i^z e_j^z - (1/3)\delta_{ij}) = Q_{bulk}(\delta_{iz}\delta_{jz} - (1/3)\delta_{ij})$, where $\boldsymbol{e}^z$ is a unit vector parallel to the z-axis.

We employ the following simple relaxation equation as the equation of motion for Q_{ij}:

$$\frac{\partial}{\partial t} Q_{ij}(\boldsymbol{r}) = -\Gamma \frac{\delta F}{\delta Q_{ij}(\boldsymbol{r})}, \tag{4}$$

where F is the total free energy of the system and Γ is a kinetic coefficient, which is associated with rotational viscosity and assumed to be a constant.

We consider a simple case where rotational symmetry can be assumed and we take the z-axis as the symmetry axis, parallel to the nematic orientation at infinity. We place the center of the spherical particle of radius R_0 at the origin. As noted in the Introduction, we use a technique of adaptive mesh refinement as in our previous studies [15,16]. We first introduce a transformation $\zeta = R_0^{-1} - r^{-1}$ and prepare in the (ζ, θ) space a $L_\zeta \times L_\theta = 32 \times 64$ rectangular lattice with equal grid spacings. Mesh refinement is achieved by a sequence of up to 8 bisections in the (ζ, θ) space and our numerical system thus corresponds to $2^{13} \times 2^{14}$ non-adaptive grids. The finest grid size in real space is then approximately $(1.2\times 10^{-4}\, R_0) \times (1.9 \times 10^{-4}\, R_0)$, which allows the investigation of a defect whose size is of the order of $10^{-3}\, R_0$.

RESULTS

No External Field

In Figure 2 we show the equilibrium orientation profiles and the corresponding numerical grids under no external field ($\tilde{H} = 0$) for $\xi = 2 \times 10^{-3}$ and $\xi = 1.85 \times 10^{-2}$. These results indicate that both the hedgehog and the Saturn ring configurations are stable or at least metastable for these ξ's. The equilibrium profile of a hedgehog in the case of $\xi = 1.85 \times 10^{-2}$ clearly indicates that a hedgehog is not point-like but made up of a small ring (although the fine structure of a hedgehog for

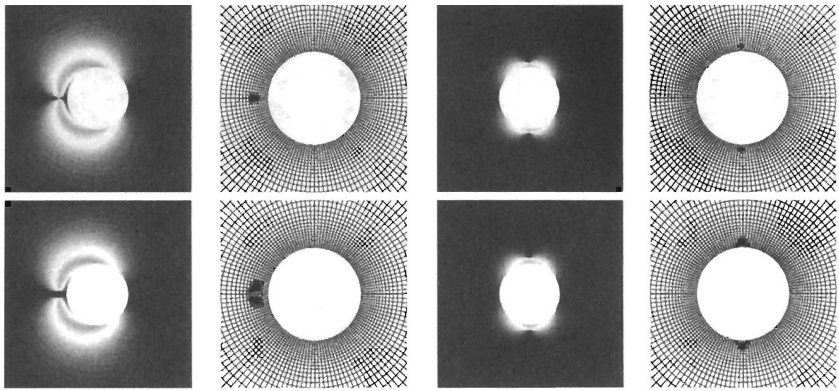

FIGURE 2 Orientation profiles (gray-scale plots of Q^2_{zz}, first and third columns) and the corresponding numerical grids (second and fourth). The first row indicates the results for $\xi = 2 \times 10^{-3}$ and the second for $\xi = 1.83 \times 10^{-2}$ Both the hedgehog (first and second columns) and Saturn ring (third and fourth) configurations are numerically reproduced as equilibrium structures.

$\xi = 2 \times 10^{-3}$ is not clear from Figure 2, a magnified view reveals that it is also a ring, not a point, as has already presented in Reference [16]). Detailed argument on the properties of a Saturn ring configuration will be given in a future article. We also note that finer grids cover the defect regions. When defect size is larger (i.e., larger ξ), the region covered by finer grids is also larger. Although it is not clear from Figure 2, the size of the finest grids is smaller for smaller ξ, because stronger spatial variation of the orientational order parameter is allowed when ξ is smaller.

When we take larger ξ, a hedgehog configuration becomes unstable to a Saturn ring. We show in Figure 3 how a hedgehog transforms to a Saturn ring for $\xi = 1.93 \times 10^{-2}$. Notice that the finer numerical grids can trace the motion of the defect and it demonstrates that our numerical scheme can be applied to the investigation of dynamics as well as statics. Instability of a hedgehog for large ξ observed here is consistent with previous theoretical and numerical studies [10,12].

Under an External Field

Transformation of a hedgehog to a Saturn ring under the application of an external field parallel to the symmetry axis has been predicted by Stark [12] and observed in a recent experiment [17]. In Figure 4 we show our simulation results as to how a hedgehog transforms to a Saturn ring under an external field. The external field is parallel to the symmetry axis (or the

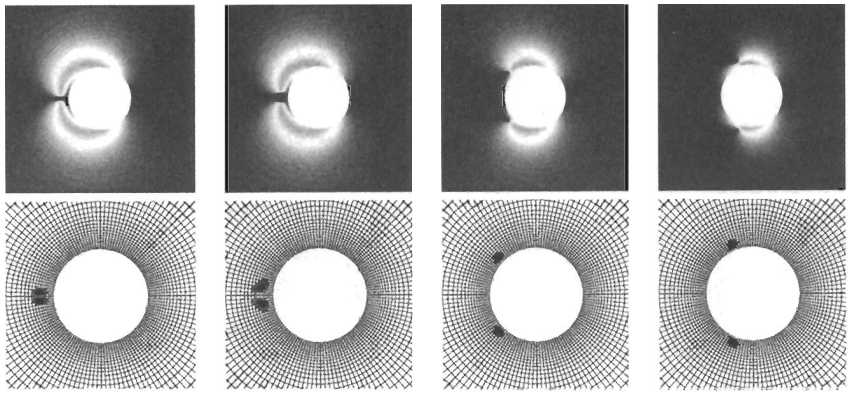

FIGURE 3 Time evolution of orientational profile (gray-scale plots of Q^2_{zz}, first row) and the corresponding numerical grids (second row) for $\xi = 1.93 \times 10^{-2}$. First column: $t = 0$, second: $5357/\Gamma A$, third: $13393/\Gamma A$, fourth: $26786/\Gamma A$. The initial configuration is the equilibrium hedgehog for $\xi = 1.63 \times 10^{-2}$.

nematic orientation far from the particle), that is, $\tilde{H}_z = \tilde{H}$ and $\tilde{H}_x = \tilde{H}_y = 0$. Notice that in the simulations of Figure 4 we have chosen $\xi = 1.07 \times 10^{-2}$, for which a hedgehog configuration is stable under no external field. We set the equilibrium configuration of a hedgehog as the initial conditions.

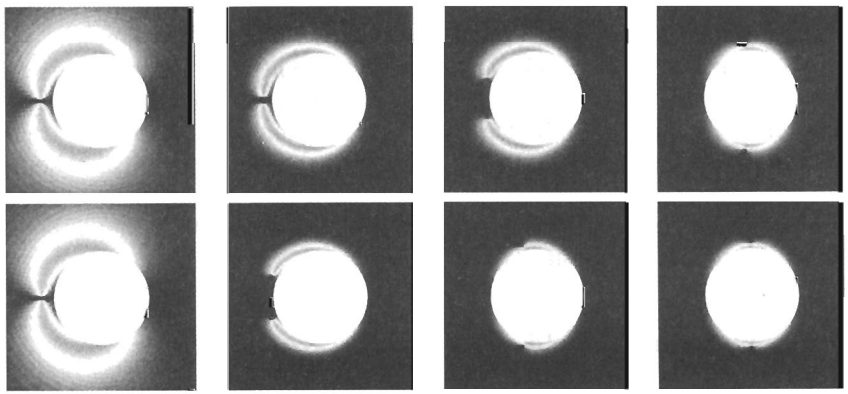

FIGURE 4 Time evolution of the orientation profile (gray-scale plots of Q^2_{zz} for $\xi_H{}^{-1} = 3.16$ (first row) and $\xi_H{}^{-1} = 5$ (second row). First column: $t = 0$, second: $t = 1875/\Gamma A$, third: $t = 4688/\Gamma A$, fourth: $t = 14063/\Gamma A$. The nematic coherence length is $\xi = 1.07 \times 10^{-2}$.

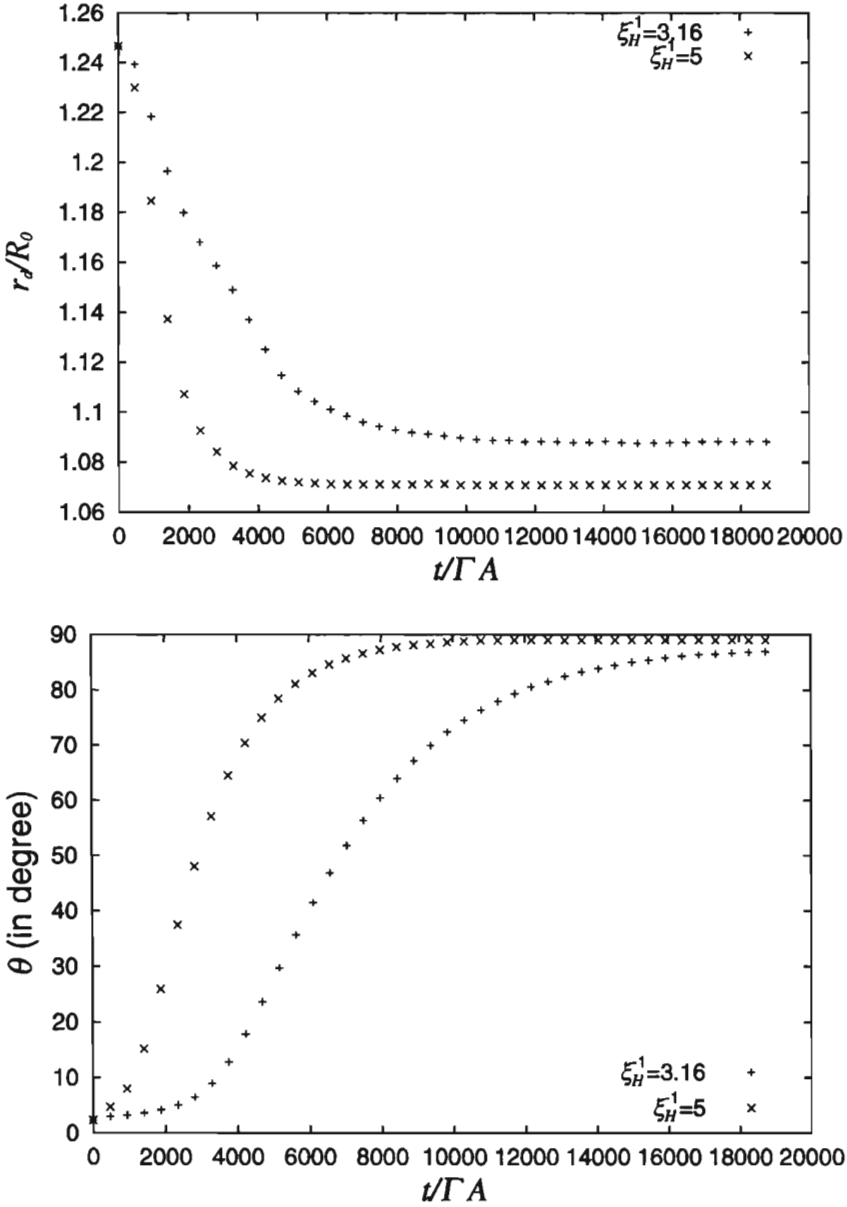

FIGURE 5 Time evolution of the defect position (r_d,θ) for $\xi_H{}^{-1} = 3.16$ and 5. Notice that $\theta \simeq 0°$ and $\theta = 90°$ correspond to a hedgehog and a Saturn ring, respectively.

Figure 4 clearly indicates that the transformation becomes faster with larger ξ_H^{-1} (or larger $\tilde{H}$). To check the transformation process more quantitatively, we plot in Figure 5 the time evolution of the defect position, which is specified by (r_d, θ). The faster transformation for larger ξ_H^{-1} can be observed also in Figure 5. Moreover, it can be seen from Figure 5 that the defect becomes closer to the particle for larger ξ_H^{-1}. This tendency can be understood intuitively as follows: to minimize the energy due to the external field the director must be aligned along the field in a larger region. A larger aligned region can be achieved when the defect goes closer to the particle. We also note that the instability of a hedgehog under an external field can be understood along the same way (notice from Figure 4 that the aligned region is larger for a Saturn ring than a hedgehog). We also observe in Figure 5 that for smaller $\xi_H^{-1}(= 3.16)$, approach of the hedgehog defect to the particle (decrease of r_d) occurs first, followed by a transition to a Saturn ring (increase of θ). This behavior might be observed in a carefully controlled experiment.

CONCLUSION

We have investigated the orientation profile and defect structure of a nematic liquid crystal around a spherical particle. Numerical implementation of an adaptive mesh refinement scheme proves to be quite a useful and powerful method to overcome a difficulty arising from the coexistence of two largely different characteristic lengths: the particle radius and the size of the defect core. Both of the experimentally observed defect structures, a hedgehog and a Saturn ring, have been successfully obtained numerically as equilibrium structures in the case of strong homeotropic anchoring on the particle surface. A transition from a hedgehog to a Saturn ring has also been observed when the defect core size is relatively large. We emphasize that to our knowledge this is the first numerical simulations which reproduce a dynamical transition from a hedgehog to a Saturn ring in a three-dimensional system.

We have also investigated how the presence of an external field affects the structure of a topological defect. We have reproduced the dynamics of the transition from a hedgehog to a Saturn ring under an external field parallel to the axis of rotational symmetry, which was observed in a recent experiment. We have found that the transition to a Saturn ring is faster under a stronger external field. Approach of a hedgehog to the particle before opening up to a Saturn ring has also been observed. Much remains to be investigated on the effect of external perturbations on the orientational configuration of a nematic liquid crystal around a particle, which will be one of the subjects of our future studies.

REFERENCES

[1] Poulin, P. *et al.* (1994). *J. Phys. II (France)*, *4*, 1557.
[2] Poulin, P. *et al.* (1997). *Science*, *275*, 1770.
[3] Meeker, S. P. *et al.* (2000). *Phys. Rev. E*, *61*, R6083.
[4] Poulin, P. & Weitz, D. A. (1998). *Phys. Rev. E*, *57*, 626.
[5] Mondain-Monval, O. *et al.* (1999). *Eur. Phys. J. B*, *12*, 167.
[6] Gu, Y. & Abbott, N. L. (2000). *Phys. Rev. Lett.*, *85*, 4719.
[7] Burylov, S. V. & Raikher, Y. L. (1994). *Phys. Rev. E*, *50*, 358.
[8] Kuksenok, O. V., Ruhwandl, R. W., Shiyanovskii, S. V., & Terentjev, E. M. (1996). *Phys. Rev. E*, *54*, 5198.
[9] Ruhwandl, R .W. & Terentjev, E. M. (1997). *Phys. Rev. E*, *56*, 5561.
[10] Lubensky, T. C., Pettey, D., Currier, N., & Stark, H. (1998). *Phys. Rev. E*, *57*, 610.
[11] Shiyanovskii, S. V. & Kuksenok, O. V. (1998). *Mol. Cryst. Liq. Cryst.*, *321*, 45.
[12] Stark, H. (1999). *Eur. Phys. J. B*, *10*, 311.
[13] Billeter, J. L. & Pelcovits, R. A. (2000). *Phys. Rev. E*, *62*, 711.
[14] Andrienko, D., Germano, G., & Allen, M. P. (2001). *Phys. Rev. E*, *63*, 041701.
[15] Fukuda, J. & Yokoyama, H. (2001). *Eur. Phys. J. E*, *4*, 389.
[16] Fukuda, J., Yoneya, M., & Yokoyama, H. (2002). *Phys. Rev. E*, *65*, 041709
[17] Loudet, J. C. & Poulin, P. (2001). *Phys. Rev. Lett.*, *87*, 165503.